ACS APPLIED MATERIALS & INTERFACES

Research Article

www.acsami.org

Pyrolyzed Carbon Film Diodes

Kirstin C. Morton,[†] Hideo Tokuhisa,[‡] and Lane A. Baker*,[†]

[†]Department of Chemistry, Indiana University, 800 E. Kirkwood Avenue, Bloomington, Indiana 47405, United States

[‡]Flexible Electronics Research Center, National Institute of Advanced Industrial Science and Technology (AIST), Central 5, 1-1-1 Higashi, Tsukuba, Ibaraki 305-8565, Japan

Supporting Information

ABSTRACT: We have previously reported pyrolyzed parylene C (PPC) as a conductive carbon electrode material for use with micropipets, atomic force microscopy probes, and planar electrodes. Advantages of carbon electrode fabrication from PPC include conformal coating of high-aspect ratio micro/nanoscale features and the benefits afforded by chemical vapor deposition of carbon polymers. In this work, we demonstrate chemical surface doping of PPC through the use of previously reported methods. Chemically treated PPC films are characterized by multiple spectroscopic and electronic measurements. Pyrolyzed parylene C and doped PPC are used to construct diodes that are examined as both p−n heterojunction and Schottky barrier diodes. Half-wave rectification is achieved with PPC diodes and demonstrates the applicability of PPC as a conductive and semiconductive material in device fabrication.

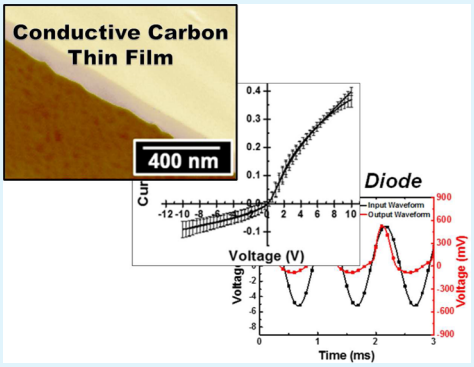

KEYWORDS: *carbon thin films, half-wave rectifier, chemical doping, amorphous conductive carbon, Schottky diodes, p−n junction diodes*

INTRODUCTION

Future prospects of electronic devices rely on miniaturization and advancement of new materials that possess properties, such as transparency and flexibility. Carbon materials (e.g., p- or n-type graphene and single-walled carbon nanotubes (SWCNTs)) have been used as replacements for or in conjunction with metal semiconductors in devices such as rectifiers,[1] diodes,[2−6] and field effect transistors (FETs).[3,4] However, these well-defined carbon materials can be difficult to prepare, manipulate, or both. Further, the superior physical and electronic properties the materials demonstrate, such as high electron and hole mobilities[7,8] and high current carrying ability,[9,10] may not be necessary for certain applications. Pyrolytic carbons are a class of disordered graphitic materials usually formed through gas phase dehydrogenation of hydrocarbon precursors. Despite long-range disorder, pyrocarbons exhibit good electrical conductivity and acceptable durability.[11] Pyrolytic carbon materials have been used previously as replacements for metals in semiconductor devices, which includes nanoscale vertical interconnect structures[12] and gate electrodes.[13]

Pyrolyzed parylene C (PPC) is a pyrocarbon utilized recently as a three-dimensional conductive carbon electrode material for nanopipettes[14] and atomic force microscopy probes.[15] However, little investigation of pyrocarbon chemical doping has been explored and investigations of pyrolytic carbon, as a component in semiconductor devices are limited. Pyrolyzed parylene C is an excellent material to construct not only planar semiconductor devices but also three-dimensional electrodes. Pyrolyzed parylene C film thickness can be tuned from roughly 200 nm to several mm, and PPC can be used to compare end-on and side-on nanoscale contact geometries[16] and to study fundamental electron transport in doped carbon materials.

In this work, we describe diodes formed between a carbon (PPC) and a semiconductor (n-type silicon) interface, likely through a Schottky barrier. Carbon has a distinct advantage over metals used in silicon-based Schottky diodes as metals often form silicides at the silicon interface, which raises the barrier height (ϕ_B).[17] Lower barrier height in a Schottky diodes means lower voltage is required to produce current in the forward-bias direction and results in lower power loss across the diode. Recently, pyrolyzed photoresist films (PPF) have been shown to function as the 'metal' in Schottky barrier diodes.[18] In this work, a ϕ_B of 0.72 eV was measured for Schottky diodes formed between PPF and n-type silicon.[18] The lowest reported ϕ_B between silicon and a pyrocarbon is 0.46 eV,[19] a value higher than the typical value for a commercially available all-silicon diode (~0.40 eV),[20] which is undesirable. In both experiments, high temperature processing was required, which limits the use of these pyrocarbons on substrates that cannot withstand high temperatures, such as polyimide or polyethylene terephthalate. Although our method to pyrolyze parylene C relies on high temperatures as well, we overcame this issue by lifting-off PPC films from copper substrates with a mild etchant, similar to methods reported for the manipulation of graphene.[21−23]

Received: July 11, 2013
Accepted: October 3, 2013
Published: October 3, 2013

To further investigate PPC as a carbon material in devices, PPC thin films were chemically treated and a p−n heterojunction diode, comprised of p-type PPC and n-type silicon, was attempted. In this device, a p−n junction diode is presumably formed at the interface between a p-type and an n-type semiconductor. Fundamental characteristics of chemically doped PPC were examined to ascertain the viability of future semiconductor devices besides diodes that could be constructed, such as flexible or transparent FETs. PPC thin films were chemically doped with nitric acid and hydrazine through strategies previously used for graphene[21,24,25] and SWCNTs.[26−31] As previously reported, nitric acid and hydrazine chemical treatments have been performed with very well-ordered carbons that were monolayers or several monolayers in thickness. In work discussed here, chemical treatments may only affect the first several PPC surface layers and chemical modifications to PPC are considered from the perspective of surface doping.

Doped PPC, characterized by photoelectron emission spectroscopy (PES), X-ray photoelectron spectroscopy (XPS) and Raman spectroscopy was used in diode construction. Electrical characteristics of junction diodes were measured and alternating current (ac) half-wave rectifiers were constructed from PPC diodes.

EXPERIMENTAL SECTION

Materials. Dichloro-[2,2]-paracyclophane (parylene C dimer) was used as received (SCS Coatings, Indianapolis, IN). Ethyl acetate (Macron Fine Chemicals, Center Valley, PA), 0.5 M ammonium persulfate (>98%) (Sigma-Aldrich, St. Louis, MO), and 3M copper conductive tape (Ted Pella, Redding, CA) were used to create lifted PPC films. Pyroylzed parylene C thin films and n-doped silicon wafers (AKI Corporation, Marumori, Yamaguchi, Japan) were cleaned with ethyl alcohol (Pharmco-AAPER, Brookfield, CT), isopropyl alcohol (IPA) (Macron Fine Chemicals, Center Valley, PA), or both. Hydrazine (0.1 M) in tetrahydrofuran (THF) (Sigma-Aldrich, St. Louis, MO) was used to chemically n-dope PPC films. Concentrated nitric acid (Mallinckrodt Chemicals, Phillipsburg, NJ) was used to create p-type PPC thin films. Poly(dimethyl siloxane) (PDMS) (Sylgard 184, Dow Corning (Midland, MI)) and contact-mode, silicon atomic force microscopy (AFM) probes (CSC17/no Al, MikroMasch USA, Lady's Island, SC) were used as received for atomic force microscopy (AFM) characterization.

Preparation of Pyrolyzed Parylene C Electrodes. Copper tape was immersed in ethyl acetate for 30 min to remove the adhesive film. Silicon substrates were washed with IPA and dried under a flow of nitrogen prior to chemical vapor deposition (CVD). Pyrolyzed parylene C was prepared, as described previously.[14,15] Briefly, CVD of parylene C onto silicon or copper was carried out in a commercial deposition system (Labcoater 2/PDS 2010, SCS Coatings), with 0.5−1.0 g of dimer used per run. Parylene C films were pyrolyzed on substrates in a tube furnace (Lindberg, Riverside, MI) at 900 °C for 1 h under constant flow of nitrogen to yield films of approximately 169 nm ± 30 nm (N = 3), measured via AFM. Pyrolyzed parylene C coated copper substrates were soaked in 0.5 M $(NH_4)_2S_2O_8$ until the copper substrate was etched sufficiently to detach the PPC film (see optical photographs of the process in the Supporting Information (SI), Figure S1).[22] Films were washed with ethanol and then water to remove any residual salts. Finally, films were transferred onto a desired substrate (e.g., polyimide, silicon, quartz, etc.) and left to air-dry at room temperature. To create PPC-silicon diodes, n-type silicon wafers (n-type ⟨100⟩, measured work function (ϕ) = 4.83 eV, number of dopant atoms (N_a) = 2.5*10^{16} atoms/cm^3) were used. More detail is provided in the SI. Both pristine and doped thin films were characterized with equipment and parameters described in the SI.

Chemical Doping of PPC Thin Films. Chemical doping of PPC thin films was inspired by previously established methods for doping of graphene and carbon nanotubes.[26,27,29,31,32] Chemically surface doped p-type PPC films were prepared by application of concentrated nitric acid to the film for 1 h. Nitric acid was then removed with a pipette and films were washed with ethanol and water. To surface n-dope PPC films, 1 M hydrazine in THF was applied to films and allowed to remain on the films for 1 h under an inert atmosphere. Hydrazine in THF was removed and films were cleaned with ethanol and water. All chemically treated PPC films were dried for several hours in air at room temperature.

RESULTS AND DISCUSSION

PPC Thin Film Characterization. To create thin film PPC materials, lift-off and transfer procedures described in the Experimental section were employed (Figure 1). Ammonium

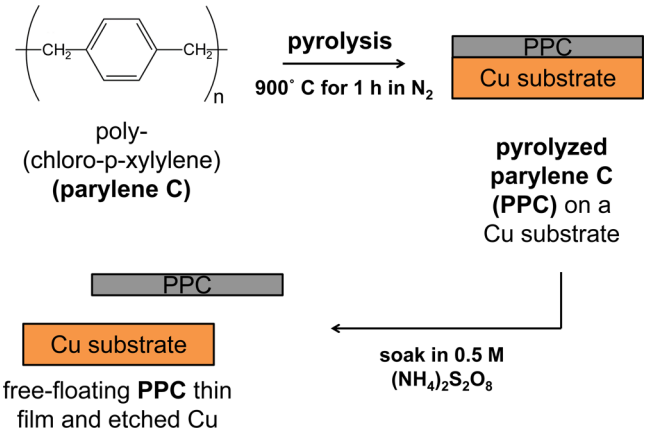

Figure 1. Schematic for thin film pyrolyzed parylene C (PPC) preparation. Parylene C is deposited onto a copper substrate via chemical vapor deposition and pyrolyzed at 900 °C under N_2 flow for an hour. The PPC thin film is removed from the copper substrate by submersion in 0.5 M $(NH_4)_2S_2O_8$ for 1−2 h, until the underlying substrate is etched away. The free-floating PPC thin film then can be cleaned and/or put onto a new substrate.

persulfate was used to etch copper because less salt residue was observed on the PPC film, via contact-mode AFM and SEM (data not shown), as compared with the use of a dilute nitric acid etchant. An optical image of the PPC film "lift-off" procedure is shown in SI Figure S1. Once the PPC film detached from the etched copper substrate, the film was cleaned and transferred to a secondary substrate, such as a flexible plastic substrate. PPC film thickness and quality were investigated for films transferred to a silicon substrate via contact-mode AFM and SEM (SI Figure S2a, b, and c). Film thicknesses were determined from average height profiles of each film sample and were found to be 169 ± 30 nm (N = 3) (SI Figure S2b). Ripples are evident in the AFM image and corresponding line profile. We hypothesize these periodic strip patterns are from a reconstruction of the underlying copper substrate, which recently has been shown to form partial dislocations at high temperatures due to strain of an overlying carbon film.[33] The roughness (root-mean-square (RMS)) value for the film on silicon in SI Figure S2a was found to be ∼21 nm for a 290 μm^2 area. From SEM (SI Figure S2c) the film appears hole-free as well, over approximately a 319 μm^2 area.

Chemical Doping of PPC Thin Films. Doped p- and n-type PPC films were prepared by drop-casting concentrated nitric acid and 0.1 M hydrazine, respectively, onto the film surface (see experimental section for details). Resistivity and work function values were measured (Table 1). Resistivity

Table 1. Work Function and Resistivity Values of Pristine, p-type and n-type PPC Films

work function (eV) of PPC		resistivity (Ω·m) of PPC
pristine	5.10	$2.08 \times 10^{-3} \pm 1.90 \times 10^{-4}$
p-type	5.30	$7.93 \times 10^{-4} \pm 1.97 \times 10^{-4}$
n-type	4.68	$5.39 \times 10^{-4} \pm 6.04 \times 10^{-5}$

values ($2.08 \times 10^{-3} \pm 1.90 \times 10^{-4}$ Ω·m (N = 5 films)) for pristine PPC were at least 2 orders of magnitude higher than the resistivity values obtained for recently reported pyrocarbons (undoped) used to create Schottky barrier diodes.[12,18] The high resistivity of pristine PPC is possibly due to the mechanical transfer of PPC films to the substrate. However, the resistivity for both p- and n-type PPC films ($7.93 \times 10^{-4} \pm 1.97 * 10^{-4}$ Ω·m and $5.39 \times 10^{-4} \pm 6.04 * 10^{-5}$ Ω·m (N = 5 films), respectively) is 2 orders of magnitude smaller than the pristine film, which suggests surface doping through increased film conductivity. The resistivity of n-type PPC is slightly lower than for p-type PPC, although both are comparable, which is consistent with the trend for SWCNTs chemically doped with HNO_3 and hydrazine previously reported.[31] Work function values found for chemically treated PPC films were found from the incident photon energy (ionization potential) from the photoelectron (PES) shown in SI Figure S3. There is some inherent error with determining the work function from PES in air in that the presence of a thick oxide layer on top of the film of interest can produce deviations in the spectra, specifically regions of nonlinearity on the curve after the onset potential. However, there is no deviation in linearity of curve after the onset potential in PES spectra in SI Figure S3, which suggests little influence of any oxide layer present. From PES spectra, the work function was found to be 5.30 and 4.68 eV for p- and n-type films, respectively. A shift of ca. +0.20 eV for p-doped PPC films and −0.42 eV for n-doped PPC films from the work function value (ϕ = 5.10 eV) for pristine PPC was observed. Thus, PES measurements acquired in air show relative shifts in work function for p- and n-type films, compared to the pristine sample, and further suggest surface doping. Yet, work function and resistivity values do not conclusively demonstrate the mechanism of doping (i.e., whether molecules are bonded covalently or are physisorbed to the film). X-ray photoelectron spectroscopy and Raman spectroscopy measurements of the films were conducted to further investigate doping mechanisms.

Survey XPS spectra for pristine, p- and n-type PPC thin films prepared on silicon are shown in SI Figure S4. Significant peaks identified are assigned to Si 2p, Si 2s, C1s, N1s, O1s, and the O KLL Auger shells. Although the parylene C precursor contains chlorine, no significant Cl 2p peak was identified in the pristine PPC XPS survey spectra. Presence of Si 2s and Si 2p peaks are attributed to influence from the underlying silicon substrate. The C/O ratios for pristine, p- and n-type PPC were approximately 0.90, 0.90, and 0.70, respectively. From survey spectra, we also note the appearance of a nitrogen peak for chemically treated PPC samples.

High-resolution C1s XPS spectra for p-type, pristine, and n-type PPC thin films are shown in Figure 2a. Graphite is known to exhibit an asymmetric C1s XPS spectrum,[34] and the core level C1s peak observed for pristine PPC is also asymmetric. The primary C1s peak for pristine PPC at 284.6 eV is attributed to sp^2 carbon.[25,28,35] In addition, the presence of a small tail at 287−290 eV is indicative of $\pi-\pi^*$ shakeup peaks and is characteristic in the C1s spectra of carbon materials.[28,34] Peak

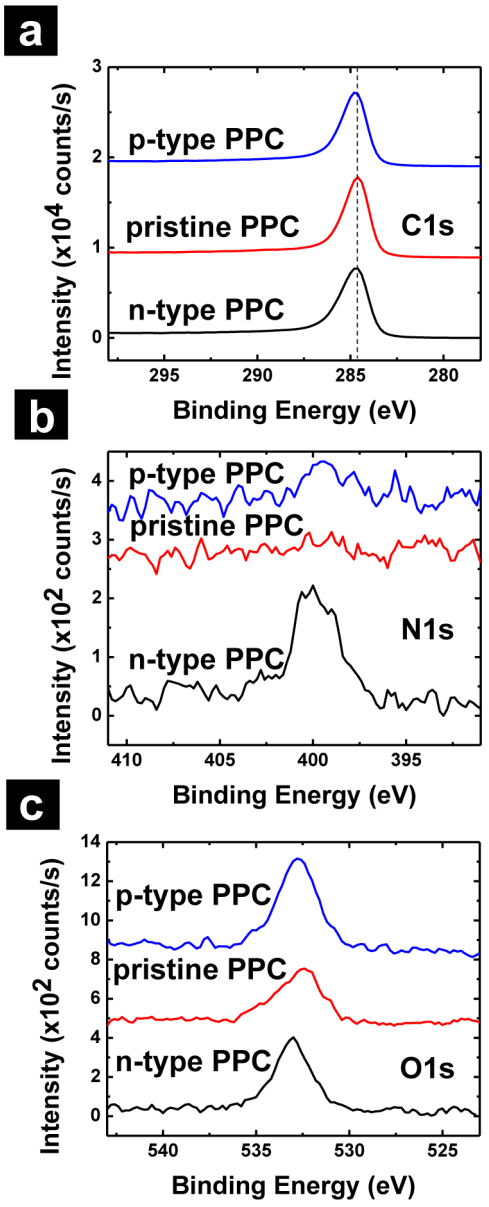

Figure 2. X-ray photoelectron spectra (XPS) for p-type, pristine, and n-type PPC thin films, prepared on n-type silicon. The high-resolution C1s (a), N1s (b), and O1s (c) spectra are shown for all three types of PPC thin films. XPS data was taken with a monochromatic Al Kα X-ray source and spectra were averaged over 10 scans.

downshifts of approximately 0.2 and 0.1 eV are noted in the main peak in the C1s XPS spectra for p- and n-type PPC films. A downshift of 0.2 eV has been reported previously for HNO_3-treated carbon nanotube films and the small shift was attributed to nitric acid desorption in a UHV environment.[29] In addition, a downshift is consistent with a shift in the Fermi level toward the valence band edge for p-type doping. An upshift of the primary peak in C1s core level spectra is expected for hydrazine-treated SWCNT samples due to the shift of the Fermi level toward the vacuum level with n-type doping. However, a small downshift of 0.2 eV for SWCNTs doped with hydrazine in THF has been reported.[25] We attribute the 0.1 eV downshift of the primary peak noted in the C1s core-level spectrum to the destabilization of hydrazine from the surface of the PPC film in UHV, which may occur more readily if the majority of N_2H_2 is physisorbed to the surface. Of note is the

absence of large, distinct peaks associated with sp^3 carbon bonding (typically found at 290−300 eV[31]) for pristine, p-type, and n-type PPC films. Thus, the primary mechanism for n-type doping is likely charge-transfer of physisorbed molecules, rather than covalent bond formation to carbon. A study of the short-term stability of pristine and chemically treated PPC films over time was also undertaken. High-resolution C1s spectra are shown for PPC thin films (SI Figure S5a). An upshift in the primary peak in the C1s spectra for pristine (284.4 eV), p-type (284.5 eV), and n-type (284.4 eV) samples was observed after storage in ambient conditions for one week. Instability of nitric-acid treated SWCNT films has been reported previously and is a known drawback of this chemical treatment.[36] Thus, the same doping instability is observed for chemically treated PPC thin films when exposed to air for one week, when exposed to a UHV environment, or both.

Spectra for high-resolution N1s scans are shown in Figure 2b. Presence of nitrogen in the n-type PPC thin films is observed, whereas the pristine PPC spectrum which does not show any discernible peaks. There may be a peak at approximately 399.4 eV in the p-type N1s spectrum, although the signal-to-noise ratio is low, which could be the result of NH_4^+ groups[37] physisorbed to the film after treatment with $(NH_4)_2S_2O_8$ and lift-off from copper substrates. However, for pristine, p-type, and n-type PPC, we cannot conclude (due to the low signal-to-noise of the peak between 399 and 400.2 eV for pristine PPC) that the chemical preparation methods used here do not contribute a significant amount of nitrogen from ammonium persulfate after lift-off from copper substrates. A N1s peak at 406−407 eV is expected in the spectrum of a p-type PPC film, as this is the range normally consistent with HNO_3 and NO_2, but this was not observed experimentally.[28] Similar absence of peaks between 406 and 407 eV in N1s XPS spectra of SWCNTs treated with concentrated nitric acid for only 1 h of treatment have been reported.[28] Thus, peaks within this range may be absent due to the short (1 h) exposure of PPC films to nitric acid or desorption of physisorbed nitrogen in UHV. In the case of n-type PPC films, a large N1s peak at approximately 400 eV was observed, which is attributed to amine groups, which likely arise from chemical treatment with hydrazine.[25,31] However, N1s peaks at ca. 400 eV have been observed for n-doped graphene sheets, and the peak observed here may be the result of pyrolytic nitrogen, embedded in the π-conjugated carbon environments of the film, as well.[38] After one week in ambient storage conditions, the large N1s core peak for n-type PPC films (400 eV) decreases in intensity (SI Figure S5b). Absence of nitrogen peaks for n-type PPC films after 1 week of aging supports the idea that chemically treated films are not stable in ambient conditions for a prolonged period of time.

Finally, high-resolution O1s spectra for pristine, p-type, and n-type PPC were investigated (Figure 2c). The presence of ambient oxygen on the film is evident from the peak (532.4 eV) shown for pristine PPC. An additional peak at 534.8 eV is also evident in the pristine PPC sample, which may be from COOH.[39] The most intense O1s core level peaks for p- and n-type PPC thin films are approximately 532.8 and 533.0 eV and correspond to C═O and C−OH, respectively.[39] A peak at approximately 532.6 eV corresponds to oxides of nitrogen, and would be expected in both p- and n-type PPC.[40] The absence of peaks at approximately 535 eV suggests there is neither chemisorbed oxygen nor adsorbed water.[41] Inspection of the O1s spectra shown in SI Figure S5c shows that peak positions all downshift to approximately 532.0, 532.0, and 532.1 eV for p-type, pristine, and n-type PPC thin films, respectively, after one week of aging in air. In addition, peaks appear more symmetric and occur at a similar binding energy, which suggests a return to same oxygen-functionality. Thus, these observations support the hypothesis that chemically treated films are not stable in ambient conditions for a week since the O1s signature for doped films becomes similar to the pristine with time.

Conclusions from XPS related to charge-transfer and the effect of surface treatment were further confirmed with Raman spectroscopy and Raman spectral mapping. Raman spectroscopy is an excellent method for the evaluation of carbon materials and also for analyzing the effects of doping as the D bands are present in sp^2 carbons with defects,[42] which can be greatly increased with n-type doping, especially. Raman spectra for pristine, n-type, and p-type PPC thin films are shown in Figure 3. The G, D, and 2D bands, typical of many carbon

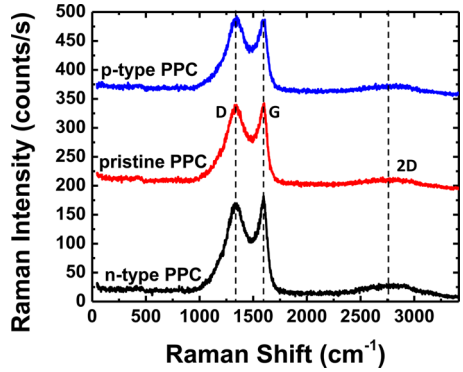

Figure 3. Raman spectra for p-type, pristine, and n-type PPC films in a given location for films prepared on quartz. The D, G, and 2D band peaks are highlighted for the pristine PPC spectrum with a dotted line for comparison to the n- and p-type.

materials, for pristine PPC are noted at approximately 1337, 1602, and 2804 cm^{-1}, respectively. The G band results from in-plane vibrations of sp^2 carbon atoms (E_{2g} symmetry group) and has often been used to describe the graphitic content of a carbon material.[40,43,44] The D band is generally believed to originate from the A_{1g} mode of small, carbon crystallites or grain boundaries of larger crystallites within the material,[44] although the exact assignment has been the subject of debate.[45] The 2D band (second order overtone of the D band) is a prominent peak in graphene and truly graphitic samples,[43] although it is weak in PPC thin films. In amorphous carbon structures the so-called Raman selection rule (wavevector (k) ≈ 0) becomes relaxed and peaks become broadened instead of sharp (as is the case in Figure 3 spectra).[46] For example, the full-width at half-maximum (fwhm) for the G and D peaks were determined to be approximately 248 and 155 cm^{-1}, which is much broader than peaks found for graphene films.[35,43] The broad 2D peaks observed (Figure 3) also make identification of this exact peak position and fwhm challenging.

Doping effects in carbon materials are often noted in Raman spectroscopy,[25,27,28,31,32,35,38,47] especially through comparison of D, G, and 2D peak shifts and peak intensity ratios. At a laser excitation of 532 nm (2.33 eV), the D, G, and 2D peaks of p-type PPC occur at 1346, 1608, and 2831 cm^{-1} and have FWHMs of approximately 248 and 155 cm^{-1} for D and G bands, respectively (Figure 3). The D, G, and 2D bands in the n-type PPC Raman spectrum are found at 1330, 1596, and 2807 cm^{-1} and the fwhm for these D and G bands are ∼271

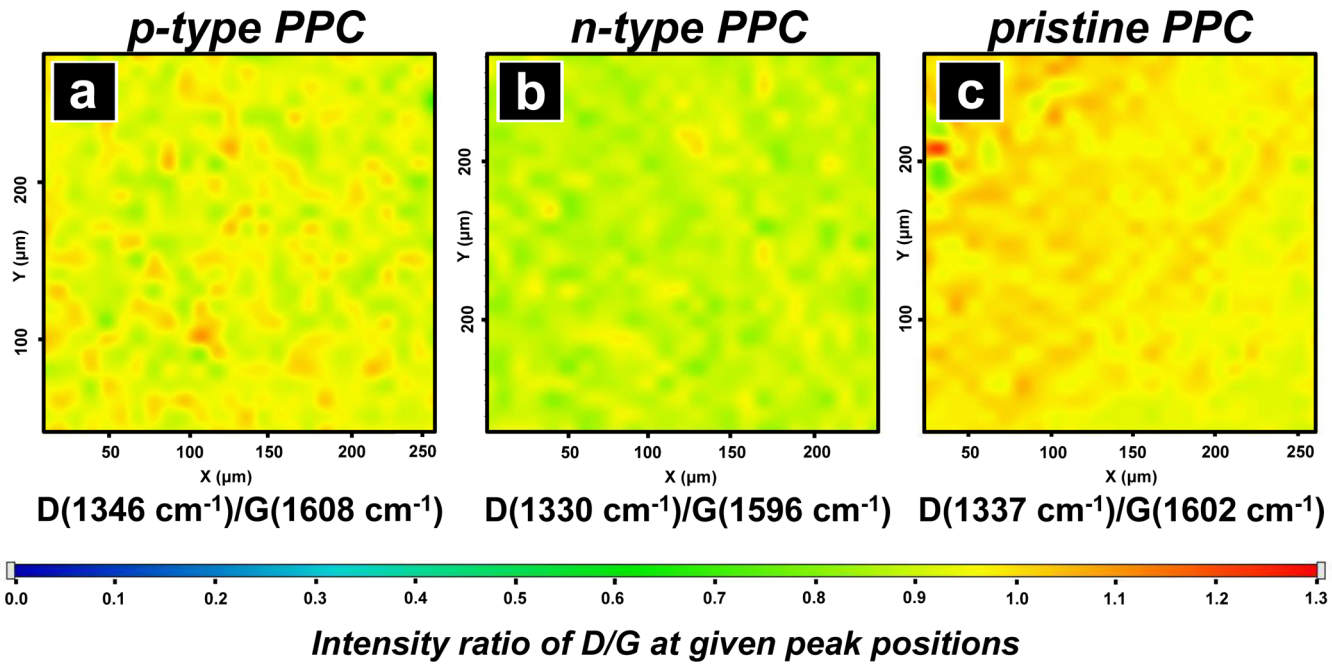

Figure 4. Raman spectral mapping for p-type (a), n-type (b), and pristine (c) PPC for an approximately 250 × 250 μm^2 area for the same samples shown in Figure 3. Raman spectra mapping shows the ratio of D to G band peaks across three samples.

and 136 cm^{-1} (Figure 3). As in the case of pristine PPC thin film Raman spectra, we found the fwhm difficult to determine in the doped PPC sample spectra due to the low S/N ratio of the 2D peak. We note there is a small, but observable red-shift of the G band of about 6 cm^{-1} for hydrazine-treated PPC films and a G band blue-shift of about 6 cm^{-1} for the nitric-acid treated PPC films, compared to the pristine PPC peak position. However, we note that the intensities of both the D and G bands for p-type, pristine, and n-type PPC are quite similar. Yet, the peak shifts observed confirm hydrazine chemical treatment makes the PPC film strongly n-type through the donation of electrons, which shifts the Fermi level toward the conduction band, and that nitric acid treatment makes PPC p-type by withdrawing electron density, which shifts the Fermi level closer to the valence band.

To further investigate the PPC thin films, Raman spectral mapping over a 250 × 250 μm^2 area was performed for p-type, n-type, and pristine PPC (Figure 4a, b, and c). Information about the variability of the D and G bands over a large area would provide a greater wealth of information than point Raman spectra. Despite difficulties in the assignment of D and G peak positions on a given spectrum due to peak broadening, we mapped the intensity ratio of the D and G bands (I_D/I_G) for each sample. The I_D/I_G ratio can reveal in-plane and edge defects in carbon materials (i.e., the relative disorder and order within a carbon sample). In addition, the I_D/I_G ratio can reveal topological defects from doping, especially in the case of n-type carbon materials, where nitrogen insertion into the sp^2 matrix can induce defects.[45] Therefore, the I_D/I_G value was plotted as color gradations in the Raman spectral mapping experiments for 10 μm step sizes. The color scale in Figure 4 represents I_D/I_G from 0 to 1.3 and each sample has been normalized to the same scale. For $I_D/I_G > 1$, we can conclude the area contains significant defects and for $I_D/I_G < 1$, more graphitic or ordered carbon content is present. The pristine PPC sample appears to have large areas of defects and some areas where $I_D/I_G \sim 1$. From the Raman spectral map for n-type PPC, we noted that I_D/I_G is less than 1 ($\sim$ 0.7 throughout) and conclude that there appears to be more graphitic content than for the pristine sample. The Raman spectral map for p-type PPC shows isolated areas with $I_D/I_G \leq 0.9$ intermixed with regions where $I_D/I_G \geq 1.0$. Previously, Raman spectral studies of n-doped graphene[32] and one type of amorphous carbon[48,49] have shown an increase in the D band intensity with doping, relative to the G band intensity, as compared to the pristine sample, which is opposite to the trend we observed here. Most likely, the pristine PPC films in this work are characteristic of a carbon between nanocrystalline graphite and low sp^3 amorphous carbon (between stage 1 and stage 2), according to the characteristics outlined by Ferrari et al.[50] Based on the inverse linear relationship between graphitic cluster size (L_a) and the I_D/I_G ratio, proposed by Tuinstra and Koenig,[44] the in-plane graphitic microcrystalline size in the PPC film appears to increase with doping from the trend observed in Figure 4. However, Cho et al. observed that when the I_D/I_G ratio is above 1.1 for amorphous carbons, which is seen in the Raman spectral maps for pristine PPC, the Tuinstra and Koenig trend no longer holds.[51] The failure of the relationship can be attributed to carbons where L_a is extremely small and there are a small number of crystallites.[50,52] Ferrari and Robertson previously showed that the development of a D peak indicates order in amorphous carbons, which is opposite to the trend observed in graphite.[50] Thus, we hypothesize that the decrease of the I_D/I_G ratio is due to a decrease in I_D with respect to I_G (since the strength of the D band is proportional to the crystallite area for small L_a[50] and the G band is simply a measure of sp^2 carbon vibration) when the film is doped.

PPC/Silicon Schottky Diode Fabrication and Electrical Characterization. Fabrication of pristine PPC/n-type Si diodes is detailed in the SI. Both Schottky and p−n junction diodes can be described by the *ideal diode equation*,[53]

$$I = I_s(e^{qV/nk_BT} - 1) \quad (1)$$

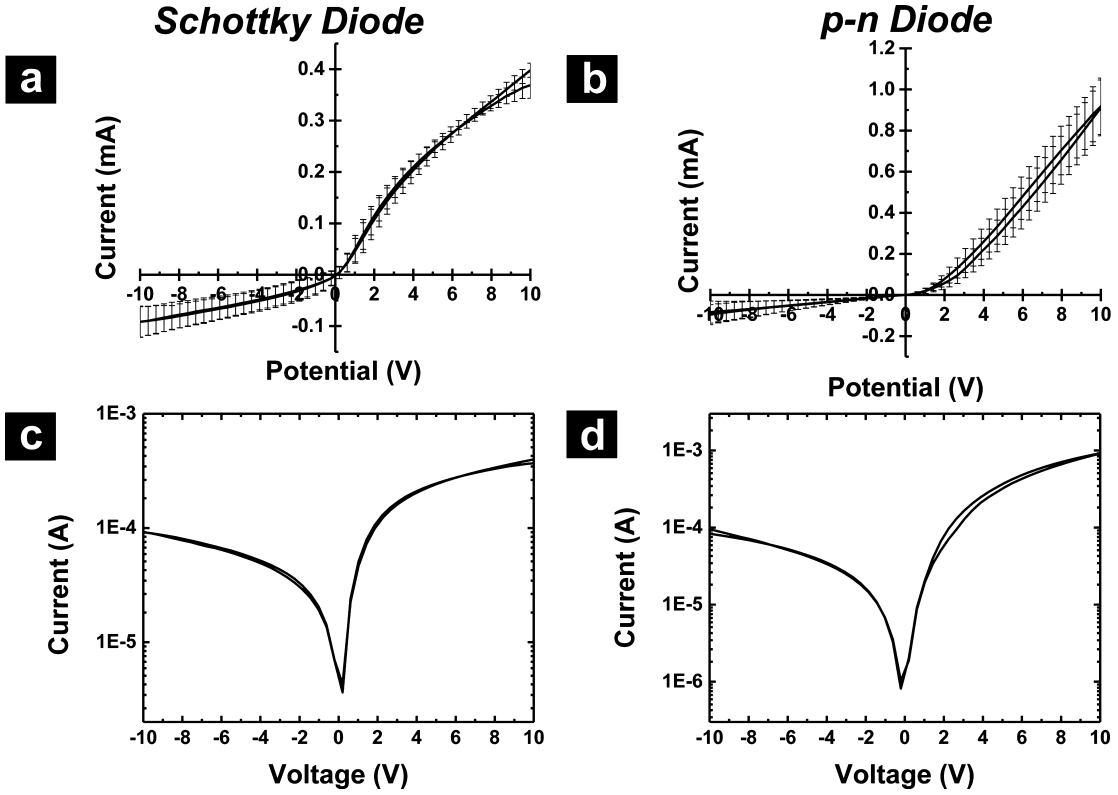

Figure 5. Current−voltage (I−V) curves for constructed Schottky barrier (a) and p−n junction (b) diodes. Error bars are shown for N = 3 diodes with measurements performed at room temperature. The current axis of the I−V curves in (a) and (b) is shown as a log-scale in (c) and (d), respectively. p−n heterojunction diodes were made from p-type PPC and n-type silicon. Schottky diodes were made from pristine PPC and n-type silicon.

where I is current, I_s is the reverse-bias saturated leakage current, q is fundamental electron charge, V is voltage applied, k_B is Boltzmann's constant, T is temperature, and n is the ideality factor for a given diode material. The ideality factor is assumed to be unity, but it usually is much larger.[54] Many of these parameters can be found experimentally from current−voltage (I−V) curves of the device.

Averaged I−V curves for fabricated Schottky diodes (N = 3 diodes), are shown in Figure 5a. A positive bias was applied to the PPC film and a negative bias was applied to the n-type silicon substrate with a voltage range of ±10 V. The I−V curve behavior between different devices was in good agreement and suggests reproducibility of the preparation method. The PPC/n-type silicon assembly shows a rectified I−V curve (Figure 5a), characteristic of a diode. In contrast, the I−V curve for a PPC film shows no rectification (SI Figure S6). Here, we consider the current rectification ratio (R_{dc}), obtained from current−voltage curves, as the following:

$$R_{dc} = |I_+/I_-| \quad (2)$$

Where I_+ and I_- are currents at the same corresponding positive and negative applied voltages. For these devices, the average R_{dc} was approximately 4.2 (at ±4 V). The turn-on voltage for the diode, defined as the forward voltage required to conduct current through the diode greater than the leakage current in the reverse-bias regime, is approximately 1.8 V. A semilog plot of the I−V curve is shown in Figure 5c. In the reverse-bias direction, the current becomes saturated, as evident from the I−V curve in Figure 5a. The reverse-bias behavior can be noted by a gradual saturation of current in the semilog plot shown in Figure 5c. However, the reverse-bias behavior does deviate from the behavior of an ideal diode, which has a much more abrupt current saturation at reverse-bias. Deviation from ideal behavior is possibly the result of high electric fields produced by the edges of our diode, not accounted for in eqs 1 and (S1), which assume a parallel electric field on the substrate.[19]

An initial evaluation of PPC/n-type silicon diode parameters was undertaken with the Norde method.[55] An account of mathematical evaluations can be found in the SI text and Figure S7. Due to the limitations and suppositions of this model, mostly the assumption of a low series resistance (R_s), a method described originally by Cheung and Cheung[56] and undertaken by Yim et al.[18] to extract ϕ_B, n, and R_s was utilized. Further correction to obtain more accurate values of ϕ_B, n, as described by Aubry et al., were also performed.[57] With these treatments, a value of ϕ_B of 0.64 eV was extracted, in good agreement with values previously reported for hydrocarbons.[18,19] The ideality factor was determined to be 4.16, which suggests a high R_s. Based on the experimentally measured and derived parameters, a band diagram was constructed for the Schottky diode (SI Figure S8).[53] The high R_s and n could be improved with our device if the contact resistance of PPC to Si was lowered.

PPC/Silicon p−n Heterojunction Diode Fabrication and Electrical Characterization. Fabrication of p-type PPC/n-type Si diodes is detailed in the SI. A similar approach to evaluate p−n heterojunction diode parameters as described for fabricated PPC/n-type silicon diodes in the previous section was used. Forward and reverse sweeps of averaged I−V curves (N = 3 diodes) operated at ±10 V are shown in Figure 5b. A rectified I−V curve is observed when p-type PPC is biased and an R_{dc} (at ±10 V) of approximately 9.6 was determined. The

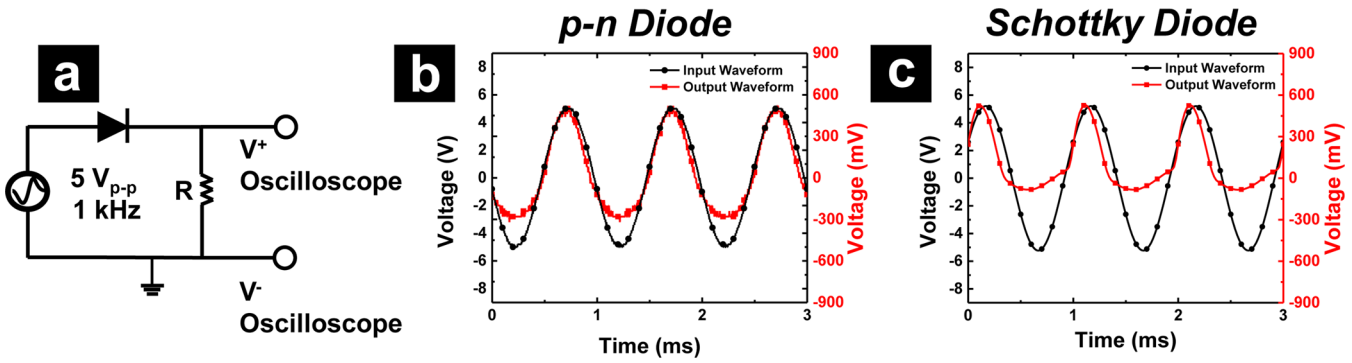

Figure 6. (a) Circuit diagram for the rectifier made through incorporation of either the p-type PPC/n-type Si diode or the PPC/n-type Si Schottky diode. A 5 $V_{p\text{-}p}$, 1kHz ac waveform was applied between ground and one of the constructed diodes. The values of the resistor (R) used in the circuit with p−n junction and Schottky diode were 2 kΩ and 4.6 kΩ, respectively. The input and output waveforms are shown for fabricated p−n heterojunction (b) and Schottky barrier (c) diodes.

turn-on voltage for the diode was approximately 2.2 V. The subtle difference in turn-on voltage between the p−n junction and Schottky diodes were used to differentiate between the two *I*−*V* curves. The turn-on voltage for the p−n junction diode is expected to be higher,[53] which was shown experimentally here. However, the small difference in turn-on voltage between the Schottky and p−n junction diode suggests that the performance of the p−n junction diode is poor. This may be the result of only chemically doping the surface of the p-type PPC film. The error bars shown for the *I*−*V* curve in Figure 5b show good reproducibility between different devices. A semilog plot of the data in Figure 5d shows a slow current saturation at high positive voltages, which is characteristic of an ideal diode (as described in eq 1). The forward-bias current levels off, which is most likely the result of surface doping, high R_s and poor contact between the n-type Si and p-type PPC. The reverse-bias current behavior, however, deviates from an ideal diode (i.e., there is not an abrupt current saturation). The device reverse-bias breakdown voltages were evaluated with a semiconductor parameter analyzer (see Experimental section). For a typical p-type PPC/n-type Si diode device, breakdown voltages were −4.67, −8.52, and −25.7 V for −10, −50, and −100 μA of anode current at the breakdown voltage, respectively. In future studies, to definitively verify the nature of the p−n junction diode, additional characterization techniques, such as a temperature-dependent *I*−*V* curves and capacitance−voltage measurements are required.

To evaluate parameters of the p-type PPC/n-type silicon diode, eq 1 was fitted to the forward-bias region of the semilog plot shown in Figure 5d. The saturation current, I_s, was determined to be 1.19 μA and *n* to be 5.46. However, *n* from eq 1 may not be reliable due to the assumption of a low R_s. For clarity, a band diagram of an idealized p-type PPC/n-type Si diode is shown in SI Figure S8. Most likely, R_s in this device is high, as noted in the fabricated PPC/n-type silicon Schottky diode, which results in a voltage-dependent *n*. Unlike a Schottky barrier diode, the charge-transport mechanisms in the forward-bias direction of a p−n junction diode can be due to many phenomena, dependent on the voltage applied and the *n*.[1,58] In the case of a SWCNT diode fabricated by Biswas et al., deviation from the ideal diode equation was seen at high forward-bias voltages due to a large R_s, which resulted in a high *n*.[1] Since the semilog *I*−*V* curve (Figure 5d) shows a similar deviation from the *ideal diode equation* at high forward-bias voltages and a high *n* is observed, a high R_s is probable. A more detailed capacitance−voltage analysis is necessary to determine additional attributes of the diode (e.g., size of a depletion region, doping density).

Half-Wave Rectifier Circuit with PPC Thin Film Diodes. Rectifiers are one important application of diodes. In this work, a simple, half-wave rectifier circuit, shown in Figure 6a, was constructed. Performance of both p-type PPC/n-type Si p−n heterojunction and PPC/n-type Si Schottky barrier diodes were evaluated as the diode represented in this circuit. Half-wave rectification of an ac waveform results in an output waveform that only exhibits current from one voltage polarity and is thus transformed to a direct current (dc). To quantify the degree of ac waveform rectification, the rectification ratio (R_{ac}) (not to be confused with the rectification ratio of an *I*−*V* curve) can be evaluated, which is defined by[59]

$$R_{ac} = |V_{out+}/V_{out-}| \quad (3)$$

where V_{out+} is the positive output circuit voltage and V_{out-} is the respective negative output voltage. A waveform of 5 $V_{p\text{-}p}$ and 1 kHz was applied in circuits with both types of devices. Resistors (noted as *R* in Figure 6a) with values of 2 and 4.2 kΩ were used in circuits that contained p-type PPC/n-type Si p−n heterojunction and PPC/n-type Si Schottky barrier diodes, respectively. The value of *R* was selected based on best half-wave rectification (ac waveform, 5 $V_{p\text{-}p}$/1 kHz) ratio found for devices. The input and output waveforms for a p-type PPC/n-type Si p−n heterojunction and PPC/n-type Si Schottky barrier diode are shown in Figure 6b and c. In both cases, the current output is much less than the input voltage, which is the result of the voltage drop across the diode. From the output response in Figure 6b, the circuit with a p-type PPC/n-type silicon diode does not show significant ac waveform rectification. Evaluation of eq 3 shows the rectification ratio to be approximately 1.9 for a circuit that contains a p-type PPC/n-type Si diode. The rectification value found from ac measurements does not agree well with the rectification ratio (approximately 9.6) of the device *I*−*V* curve (shown in Figure 5b). Discrepancy between ac and dc measurements may be the result of a voltage-dependence on R_s found with eq 3, which has been shown previously.[59] The output response for a PPC/n-type Si Schottky diode, shown in Figure 6c, shows much more significant rectification and very little current for negative input voltages. The R_{ac} value found for the rectifier circuit that contains the PPC Schottky diode is approximately 7.2, which is much higher than for the circuit with the PPC p−n junction

heterojunction diode. Also, the R_{ac} is comparable to previously reported values for rectifier circuits that contain carbon nanotubes.[1,60,61] Some distortion of the ac output waveform is noted in Figure 6c and this may be the result of a low carrier mobility relative to silicon or SWCNTs.[1] Interestingly, the value of the resistor used in the rectifier circuit should match the R_s value obtained for Schottky diodes found by fitting $I-V$ curves in the previous section. We found successful half-wave rectification with a resistor value of 4.2 kΩ, which is smaller than R_{dc} found from fitting experimental $I-V$ curves (14.6 kΩ). Kirchoff's circuit laws state that for the circuit shown in Figure 6a, in which the PPC-silicon junction and the resistor lie in series, the current flowing through this junction and the resistor are equal.[62] Thus, we can assume that experimentally in this case, the resistance of the Schottky diode is approximately the same value as the resistor used in the circuit (4.2 kΩ). Differences in these resistance values could be the result of the mathematical models used to fit the device $I-V$ curves, which assume a low series resistance across a Schottky diode and which were likely not valid for our devices.

CONCLUSIONS

In conclusion, PPC thin films were created and chemically treated to yield two types of diodes. Surface chemical doping of PPC was explored and p- and n-type PPC films were created from nitric acid and hydrazine chemical treatments, respectively. Detailed analysis of chemically doped films suggests that nitric acid is weakly adsorbed to PPC and is chemically reversible with time. Hydrazine-treated PPC films were found to be more stable both in air and UHV. In addition, chemical treatments decreased the I_D/I_G ratio, as compared to the case of pristine PPC.

Devices described demonstrate that a pyrocarbon, PPC, can be tuned to a desired thickness and transferred to an arbitrary substrate to create diodes. Pristine PPC was used with n-type silicon to create a Schottky barrier diode, which has been accomplished for pyrocarbons only in two other instances.[18,19] We found that the pristine PPC/n-type silicon Schottky barrier diode had a very high series resistance. Barriers calculated for Schottky diodes here ($\phi_B \sim 0.64$ eV) were comparable to previously reported pyrolyzed carbons.[18,19] The ideality factor for the Schottky diode and R_s were determined to be 4.16 and 14.6 kΩ, respectively. In addition, an attempt to create a p-type PPC/n-type Si heterojunction diode was undertaken. The p−n junction diode performance was poor, as noted from the low turn-on voltage in the $I-V$ curves. Also, the electrical behavior of the p-type PPC/n-type Si junction diode is not dramatically different from the electrical behavior of the pristine PPC/n-type PPC diode, which suggests that a true p−n interface may not have been formed. The ideality factor of this type of diode was found to be about 5.46, which suggests a high R_s. Both types of diodes were placed in a half-wave rectification circuit to demonstrate the applicability of the diodes. We found that the fabricated Schottky barrier diodes showed good rectification and had a R_{ac} of about 7.2, significantly higher than the R_{ac} found for the p−n heterojunction diode (∼1.9).

Overall, the creation of amorphous carbon films for transfer to a variety of substrates, the chemical treatment of the films to make n- or p-type carbon and the fabrication of diodes was demonstrated. As used here, chemical doping is likely to only influence the surface layers of the carbon film. Additionally, with the lift-off method used here, intimate contact between the p-type PPC and n-type silicon was poor, which contributed to the diminished performance of the p−n junction diode. Diode performance could be improved if chemical treatments described here pervade the entire PPC film, the PPC doping density is comparable to that of silicon or the resistance between the films is minimized. In the future, these films may find use in the construction of Schottky barrier and p−n heterojunction diodes solely from PPC (with no silicon) on flexible substrates, such as poly-(imide). Further, investigations of three-dimensional diodes from PPC-coated electrodes (such as an AFM probe) and planar surfaces provide an interesting avenue to develop future devices.

ASSOCIATED CONTENT

Supporting Information

Details of diode fabrication, physical and electrical characterization, mathematical evaluation of $I-V$ curves, calculation of physical parameters, optical images, an AFM image of the film, a SEM image of the film, a contact $I-V$ curve of pristine PPC, PES, XPS, and energy band diagrams for diodes. This material is available free of charge via the Internet at http://pubs.acs.org.

AUTHOR INFORMATION

Corresponding Author

*Tel.: 812-856-1873. Fax: 812-855-8300. E-mail: lanbaker@indiana.edu.

Notes

The authors declare no competing financial interest.

ACKNOWLEDGMENTS

Funding from the Research Corporation for Scientific Advancement and the National Science Foundation (NSF) (CHE-0847642) is greatly acknowledged. K.C.M. would like to acknowledge funding from an NSF East Asia Pacific Summer Institute fellowship (Award No. OISE-1209486) and Japan Society for the Promotion of Science Summer program award (Award No. SP12040). Part of this work was carried out through the NanoProcessing Partnership Platform and the Innovation Center for Advanced Nanodevices at AIST, and staff is gratefully thanked. Assistance and funding from the Nanoscience Characterization Facility, Dr. Yaroslav Losovyj and NSF DMR 1126394 are appreciated. Use of furnaces provided by Prof. Catherine Reck is acknowledged.

REFERENCES

(1) Biswas, C.; Lee, S. Y.; Ly, T. H.; Ghosh, A.; Dang, Q. N.; Lee, Y. H. *ACS Nano* **2011**, *5*, 9817−9823.
(2) Chan, K. K.; Silva, S. R. P.; Amaratunga, G. A. J. *Thin Solid Films* **1992**, *212*, 232−239.
(3) Javey, A.; Kim, H.; Brink, M.; Wang, Q.; Ural, A.; Guo, J.; McIntyre, P.; McEuen, P.; Lundstrom, M.; Dai, H. J. *Nat. Mater.* **2002**, *1*, 241−246.
(4) Miyajima, Y.; Shkunov, M.; Silva, S. R. P. *Appl. Phys. Lett.* **2009**, *95*, 102102−102104.
(5) Yao, Z.; Postma, H. W. C.; Balents, L.; Dekker, C. *Nature* **1999**, *402*, 273−276.
(6) Zhou, Y. X.; Gaur, A.; Hur, S. H.; Kocabas, C.; Meitl, M. A.; Shim, M.; Rogers, J. A. *Nano Lett.* **2004**, *4*, 2031−2035.
(7) Durkop, T.; Getty, S. A.; Cobas, E.; Fuhrer, M. S. *Nano Lett.* **2004**, *4*, 35−39.
(8) Novoselov, K. S.; Geim, A. K.; Morozov, S. V.; Jiang, D.; Zhang, Y.; Dubonos, S. V.; Grigorieva, I. V.; Firsov, A. A. *Science* **2004**, *306*, 666−669.
(9) Javey, A.; Guo, J.; Wang, Q.; Lundstrom, M.; Dai, H. J. *Nature* **2003**, *424*, 654−657.

(10) Murali, R.; Yang, Y.; Brenner, K.; Beck, T.; Meindl, J. D. *Appl. Phys. Lett.* **2009**, *94*, 243114−243116.
(11) McEvoy, N.; Peltekis, N.; Kumar, S.; Rezvani, E.; Nolan, H.; Keeley, G. P.; Blau, W. J.; Duesberg, G. S. *Carbon* **2012**, *50*, 1216−1226.
(12) Graham, A. P.; Schindler, G.; Duesberg, G. S.; Lutz, T.; Weber, W. *J. Appl. Phys.* **2010**, *107*, 114316−114319.
(13) Raghavan, G.; Hoyt, J. L.; Gibbons, J. F. *Jpn. J. Appl. Phys., Part 1* **1993**, *32*, 380−383.
(14) Morton, K. C.; Morris, C. A.; Derylo, M. A.; Thakar, R.; Baker, L. A. *Anal. Chem.* **2011**, *83*, 5447−5452.
(15) Morton, K. C.; Derylo, M. A.; Baker, L. A. *J. Electrochem. Soc.* **2012**, *159*, H662−H667.
(16) Leonard, F.; Talin, A. A. *Nat. Nanotechnol.* **2011**, *6*, 773−83.
(17) Maex, K.; Van Rossum, M. In *Properties of Metal Silicides*; Institution of Engineering and Technology: Stevenage, 1995.
(18) Yim, C.; McEvoy, N.; Rezvani, E.; Kumar, S.; Duesberg, G. S. *Small* **2012**, *8*, 1360−1364.
(19) Graham, A. P.; Jay, T.; Jakschik, S.; Knebel, S.; Weber, W.; Schroeder, U.; Mikolajick, T. *J. Appl. Phys.* **2012**, *111*, 124511−124516.
(20) This information was obtained from datasheets of commercially avaliable Schottky diodes.
(21) Bae, S.; Kim, H.; Lee, Y.; Xu, X.; Park, J.-S.; Zheng, Y.; Balakrishnan, J.; Lei, T.; Kim, H. R.; Song, Y. I.; Kim, Y.-J.; Kim, K. S.; Ozyilmaz, B.; Ahn, J.-H.; Hong, B. H.; Iijima, S. *Nat. Nanotechnol.* **2010**, *5*, 574−578.
(22) Jo, G.-C.; Chae, G.-S.; Hwang, Y.-S.; Kwon, O.-N.; Lee, K.-M.; Baek, K.-J.; Rhee, T.-H. Etching solution for etching Cu and Cu/Ti metal layer of liquid crystal display device and method of fabricating the same. U.S. Patent No. 6,881,679, 2005.
(23) Kim, K. S.; Zhao, Y.; Jang, H.; Lee, S. Y.; Kim, J. M.; Ahn, J. H.; Kim, P.; Choi, J. Y.; Hong, B. H. *Nature* **2009**, *457*, 706−710.
(24) Long, D.; Li, W.; Ling, L.; Miyawaki, J.; Mochida, I.; Yoon, S.-H. *Langmuir* **2010**, *26*, 16096−16102.
(25) Some, S.; Bhunia, P.; Hwang, E.; Lee, K.; Yoon, Y.; Seo, S.; Lee, H. *Chem.—Eur. J.* **2012**, *18*, 7665−7670.
(26) Bower, C.; Kleinhammes, A.; Wu, Y.; Zhou, O. *Chem. Phys. Lett.* **1998**, *288*, 481−486.
(27) Geng, H.-Z.; Kim, K. K.; So, K. P.; Lee, Y. S.; Chang, Y.; Lee, Y. H. *J. Am. Chem. Soc.* **2007**, *129*, 7758−7759.
(28) Geng, H.-Z.; Kim, K. K.; Song, C.; Xuyen, N. T.; Kim, S. M.; Park, K. A.; Lee, D. S.; An, K. H.; Lee, Y. S.; Chang, Y.; Lee, Y. J.; Choi, J. Y.; Benayad, A.; Lee, Y. H. *J. Mater. Chem.* **2008**, *18*, 1261−1266.
(29) Graupner, R.; Abraham, J.; Vencelova, A.; Seyller, T.; Hennrich, F.; Kappes, M. M.; Hirsch, A.; Ley, L. *Phys. Chem. Chem. Phys.* **2003**, *5*, 5472−5476.
(30) Kamarás, K.; Pekker, Á.; Botka, B.; Hu, H.; Niyogi, S.; Itkis, M. E.; Haddon, R. C. *Phys. Status Solidi B* **2010**, *247*, 2754−2757.
(31) Mistry, K. S.; Larsen, B. A.; Bergeson, J. D.; Barnes, T. M.; Teeter, G.; Engtrakul, C.; Blackburn, J. L. *ACS Nano* **2011**, *5*, 3714−3723.
(32) Guo, B.; Liu, Q.; Chen, E.; Zhu, H.; Fang, L.; Gong, J. R. *Nano Lett.* **2010**, *10*, 4975−4980.
(33) Tian, J.; Cao, H.; Wu, W.; Yu, Q.; Guisinger, N. P.; Chen, Y. P. *Nano Lett.* **2012**, *12*, 3893−3899.
(34) Sette, F.; Wertheim, G. K.; Ma, Y.; Meigs, G.; Modesti, S.; Chen, C. T. *Phys. Rev. B.* **1990**, *41*, 9766−9770.
(35) Jin, Z.; Yao, J.; Kittrell, C.; Tour, J. M. *ACS Nano* **2011**, *5*, 4112−4117.
(36) Jackson, R.; Domercq, B.; Jain, R.; Kippelen, B.; Graham, S. *Adv. Funct. Mater.* **2008**, *18*, 2548−2554.
(37) Yang, P.; Deng, J. Y.; Yang, W. T. *Polymer* **2003**, *44*, 7157−7164.
(38) Wei, D.; Liu, Y.; Wang, Y.; Zhang, H.; Huang, L.; Yu, G. *Nano Lett.* **2009**, *9*, 1752−1758.
(39) Kostecki, R.; Schnyder, B.; Alliata, D.; Song, X.; Kinoshita, K.; Kotz, R. *Thin Solid Films* **2001**, *396*, 36−43.
(40) Zhang, G.; Sun, S.; Yang, D.; Dodelet, J.-P.; Sacher, E. *Carbon* **2008**, *46*, 196−205.
(41) Xie, Y. M.; Sherwood, P. M. A. *Appl. Spectrosc.* **1989**, *43*, 1153−1158.
(42) Thomsen, C.; Reich, S. *Phys. Rev. Lett.* **2000**, *85*, 5214−5217.
(43) Ni, Z.; Wang, Y.; Yu, T.; Shen, Z. *Nano Res.* **2008**, *1*, 273−291.
(44) Tuinstra, F.; Koenig, J. L. *J. Chem. Phys.* **1970**, *53*, 1126−1130.
(45) Ferrari, A. C. *Solid State Commun.* **2007**, *143*, 47−57.
(46) Roy, D.; Chhowalla, M.; Hellgren, N.; Clyne, T. W.; Amaratunga, G. A. J. *Phys. Rev. B.* **2004**, *70*, 035406−035411.
(47) Zhou, W.; Vavro, J.; Nemes, N. M.; Fischer, J. E.; Borondics, F.; Kamaras, K.; Tanner, D. B. *Phys. Rev. B.* **2005**, *71*, 205423−205429.
(48) Schwan, J.; Batori, V.; Ulrich, S.; Ehrhardt, H.; Silva, S. R. P. *J. Appl. Phys.* **1998**, *84*, 2071−2081.
(49) Bhattacharyya, S.; Cardinaud, C.; Turban, G. *J. Appl. Phys.* **1998**, *83*, 4491−4500.
(50) Ferrari, A. C.; Robertson, J. *Phys. Rev. B.* **2000**, *61*, 14095−14107.
(51) Chu, P. K.; Li, L. H. *Mater. Chem. Phys.* **2006**, *96*, 253−277.
(52) Ferrari, A. C.; Basko, D. M. *Nat. Nanotechnol.* **2013**, *8*, 235−246.
(53) Hu, C. C. *Modern Semiconductor Devices for Integrated Circuits* [Online]; Prentice Hall: Upper Saddle River, 2009; http://www.eecs.berkeley.edu/~hu/Book-Chapters-and-Lecture-Slides-download.html (accessed June 1, 2012).
(54) Shah, J. M.; Li, Y. L.; Gessmann, T.; Schubert, E. F. *J. Appl. Phys.* **2003**, *94*, 2627−2630.
(55) Norde, H. *J. Appl. Phys.* **1979**, *50*, 5052−5053.
(56) Cheung, S. K.; Cheung, N. W. *Appl. Phys. Lett.* **1986**, *49*, 85−87.
(57) Aubry, V.; Meyer, F. *J. Appl. Phys.* **1994**, *76*, 7973−7984.
(58) Sze, S. M. In *Physics of Semiconductor Devices*, 2nd ed.; J. Wiley & Sons: New York, 1981.
(59) Nijhuis, C. A.; Reus, W. F.; Siegel, A. C.; Whitesides, G. M. *J. Am. Chem. Soc.* **2011**, *133*, 15397−15411.
(60) Hu, P.; Xiao, K.; Liu, Y. Q.; Yu, G.; Wang, X. B.; Fu, L.; Cui, G. L.; Zhu, D. B. *Appl. Phys. Lett.* **2004**, *84*, 4932−4934.
(61) Mallick, G.; Griep, M. H.; Ajayan, P. M.; Karna, S. P. *Appl. Phys. Lett.* **2010**, *96*, 233109−233111.
(62) Diefenderfer, A. J.; Holton, B. E. In *Principles of Electronic Instrumentation*, 3rd ed.; Thomson Brooks/Cole: Stamford, 1994.